Elusiveness of infrared critical exponents in Landau gauge Yang-Mills theories

C. S. Fischer,* R. Alkofer,† and H. Reinhardt
Institute for Theoretical Physics, University of Tübingen, Auf der Morgenstelle 14, D-72076 Tübingen, Germany
(Received 21 February 2002; published 22 April 2002)

We solve a truncated system of coupled Dyson-Schwinger equations for the gluon and ghost propagators in SU(N_c) Yang-Mills theories in Faddeev-Popov quantization on a four-torus. This compact space-time manifold provides an efficient mean to solve the gluon and ghost Dyson-Schwinger equations without any angular approximations. We verify that analytically two powerlike solutions in the very far infrared seem possible. However, only one of these solutions can be matched to a numerical solution for nonvanishing momenta. For a bare ghost-gluon vertex this implies that the gluon propagator is only weakly infrared vanishing, $D_{gl}(k^2) \propto (k^2)^{2\kappa-1}$, $\kappa \approx 0.595$, and the ghost propagator is infrared singular, $D_{gh}(k^2) \propto (k^2)^{-\kappa-1}$. For nonvanishing momenta our solutions are in agreement with the results of recent SU(2) Monte Carlo lattice calculations. The running coupling possesses an infrared fixed point. We obtain $\alpha(0) = 8.92/N_c$ for all gauge groups SU(N_c). Above one GeV the running coupling rapidly approaches its perturbative form.

DOI: 10.1103/PhysRevD.65.094008 PACS number(s): 12.38.Aw, 11.15.Tk, 12.38.Lg, 14.70.Dj

I. INTRODUCTION

It is generally accepted that the theory of strong interactions, QCD, should describe the observed phenomenon of confinement: colored objects such as quarks and gluons occur only in hadrons. A possible route for gaining more understanding of this phenomenon is the study of the infrared behavior of QCD Green's functions; for a recent review see [1]. In addition, to shed light on the fundamental properties of QCD the knowledge of these Green's functions provides the basis for a successful description of hadronic physics [1,2]. Based on the idea of infrared slavery older works on this subject assumed a strongly infrared singular gluon propagator. Recent studies based either on Dyson-Schwinger equations [3–7] or lattice calculations [8–11] in Landau gauge indicate quite the opposite: an infrared finite or even infrared vanishing gluon propagator. These two techniques are complementary in the following sense: On the one hand, Monte Carlo lattice calculations include all non-perturbative physics of Yang-Mills theories but cannot make definite statements about the very far infrared due to the finite lattice volume. On the other hand, Dyson-Schwinger equations allow one to extract the leading infrared behavior analytically and the general non-perturbative behavior with moderate numerical effort but these equations, consisting of an infinite tower of coupled nonlinear integral equations, have to be truncated in order to be manageable. As we will also see in the course of this article, the propagators of SU(2) and SU(3) Landau gauge Yang-Mills theory in Faddeev-Popov quantization coincide for these two different approaches reasonably well. Thus we are confident that our results for the qualitative features of these propagators are trustable.

Especially, these recent results on the Landau gauge propagators imply that the Kugo-Ojima confinement criterion [12–14] is satisfied (for a short summary on this topic see e.g. Ref. [15]). It is gratifying to note that no truncation to the Dyson-Schwinger equations has to be applied to arrive at this conclusion if one assumes that the involved Green's functions can be represented in the infrared by asymptotic expansions [5,7]. In Landau gauge, a sufficient condition for the Kugo-Ojima confinement criterion is that the nonperturbative ghost propagator is more singular than a massless pole in the infrared [14]:

$$D_G^{ab}(p) = -\delta^{ab}\frac{G(p^2)}{p^2}, \quad \text{with} \quad G(p^2) \overset{p^2\to 0}{\to} \infty. \qquad (1)$$

This behavior is also correlated to other aspects of Yang-Mills theories. First, the Oehme-Zimmermann superconvergence relations [16] can be derived from Ward-Takahashi identities assuming the Kugo-Ojima confinement criterion [17]. These superconvergence relations formalize a long known contradiction between asymptotic freedom and the positivity of the spectral density for transverse gluons in the covariant gauge. Second, Eq. (1) agrees with Zwanziger's horizon condition [6,18]. This amounts to Gribov's prescription to cut off the functional integral at the first Gribov horizon [19]. Noting that this horizon is a convex hypersurface in A space that surrounds the origin [20] allows one to conclude that the Dyson-Schwinger equations are not changed [18]. However, one has to note that this treatment of the functional integral is related to the resolution of an ambiguity in the solution of these equations [3,6]. Nevertheless, supplementing the Faddeev-Popov quantization with this additional constraint might not be sufficient to provide an exact solution of the problem because there exist Gribov copies within the first Gribov horizon [21].

As already stated, the obtained values for the infrared exponents of the gluon and ghost propagators depend on the employed approximation for the Dyson-Schwinger equations. Beyond the necessary truncation of this set of integral equations in numerical calculations also some approximations for the angular integrals have been used so far [3,4]. On the other hand, employing infrared expansions (without using any angular approximation) which are strictly valid only in the limit of vanishing momentum, $p^2 \to 0$, [4–7] yield also

*Email address: chfi@axion01.tphys.physik.uni-tuebingen.de
†Email address: reinhard.alkofer@uni-tuebingen.de

some quite different values for the infrared critical exponent depending on the truncation scheme. With respect to these analytical calculations the question arises whether for every extracted value of the infrared exponent the corresponding numerical solution exists also for finite values of momenta. As will be detailed in this paper a tool to overcome angular approximations is the treatment of the Dyson-Schwinger equations on a compact Euclidean four-manifold, in our case a four-torus. This allows us to answer the above question: We will see that not every analytically extracted infrared exponent can be matched to a numerical solution for nonvanishing momenta.

To make this paper self-contained we will shortly summarize truncation schemes for the gluon and ghost Dyson-Schwinger equations in flat (infinite) Euclidean space-time, which have been solved recently, in the first two sections of Sec. II. In the following section we introduce a novel truncation scheme. In Sec. III we present the Dyson-Schwinger equations formulated on the momentum grid which is the dual space to the compact four-torus. In Sec. IV we will present solutions done in otherwise exactly the same approximation scheme as previous solutions for flat space-time. The comparison to these previous solutions allows us to chose a suitable regularization and renormalization procedure. [As in previous work we adopt a modified momentum subtraction (MOM) scheme.] In Sec. IV also the solutions without any angular approximations will be discussed. The central result of this paper is: only one of two solutions allowed by the infrared analysis can be matched to a numerical solution for non-vanishing momenta. E.g. for bare vertices this implies that the gluon propagator is only weakly infrared vanishing, $D_{gl}(k^2) \propto (k^2)^{2\kappa-1}$, $\kappa = 0.595\ldots$, and the ghost propagator is infrared singular, $D_{gh}(k^2) \propto (k^2)^{-\kappa-1}$. In Sec. V we present our conclusions. Furthermore, in Appendix A we present our approximation to impose one-loop scaling of the gluon and ghost propagators in the ultraviolet. In Appendix B we discuss the influence of gluon and ghost zero modes on the solutions. The numerical methods to solve the gluon and ghost Dyson-Schwinger equations in flat Euclidean space-time will be described in Appendix C.

II. GLUON AND GHOST DYSON-SCHWINGER EQUATIONS IN FLAT EUCLIDEAN SPACE-TIME

In this section a short summary of previously employed truncation and approximation schemes for the coupled gluon and ghost Dyson-Schwinger equations [3,4] will be given first. We will also provide the underlying formula for a new truncation scheme. All these schemes include all diagrams in the ghost equation and neglect contributions from the two-loop diagrams in the gluon equation, see Fig. 1, where the full gluon Dyson-Schwinger equation of QCD is represented diagrammatically. In addition, as we will be only concerned with pure Yang-Mills theory in this paper the quark loop will be neglected. The tadpole term provides in Landau gauge only an (ultraviolet divergent) constant and will drop out during renormalization anyhow. Thus, we will effectively study the coupled system of equations as depicted in Fig. 2.

The necessary trunction of the gluon Dyson-Schwinger

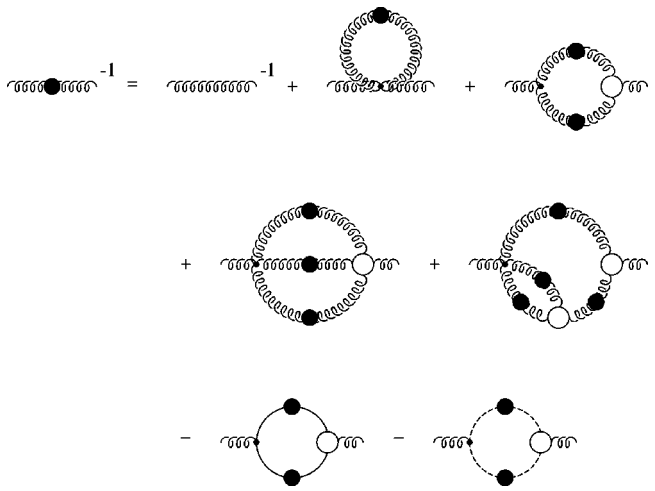

FIG. 1. Diagrammatic representation of the gluon Dyson-Schwinger equation. The wiggly, dashed and solid lines represent the propagation of gluons, ghosts and quarks, respectively. A filled blob represents a full propagator and a circle indicates a one-particle irreducible vertex.

equation immediately leads to a problem: The gluon polarization, which due to gauge symmetry would be transverse to the gluon momentum in an exact calculation, acquires spurious longitudinal terms. These terms are in general quadratically ultraviolet divergent and thus highly ambiguous because they depend on the momentum routing in the loop integral. In addition, a gauge invariant regularization scheme is required to avoid these unphysical longitudinal terms. Such schemes are, however, hard to implement in Dyson-Schwinger studies, for the corresponding use of dimensional regularization see e.g. Refs. [22,23]. An alternative unambiguous procedure is to isolate the part free of quadratic ultraviolet divergences by contracting with the projector

$$\mathcal{R}_{\mu\nu}(k) = \delta_{\mu\nu} - d\frac{k_\mu k_\nu}{k^2} = \delta_{\mu\nu} - 4\frac{k_\mu k_\nu}{k^2}, \tag{2}$$

which is constructed such that $\mathcal{R}_{\mu\nu}(k)\,\delta^{\mu\nu} = 0$, and therefore the ambiguous term proportional to $\delta_{\mu\nu}$ is projected out [24]. Note that the use of this projector also removes the tadpole term. As has become obvious recently [7] (see also Ref. [25] for a corresponding discussion in a much simpler truncation scheme) the use of the projector (2) interferes with the infra-

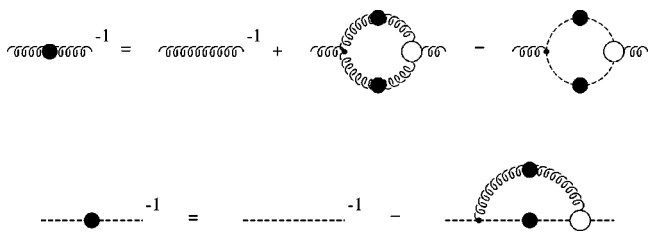

FIG. 2. Diagrammatic representation of the truncated gluon and ghost Dyson-Schwinger equations studied in this article. In the gluon Dyson-Schwinger equation terms with four-gluon vertices and quarks have been dismissed.

red analysis of the coupled gluon-ghost system. For technical reasons we will employ a one-parameter family of projectors

$$\mathcal{P}^{(\zeta)}_{\mu\nu}(k)=\delta_{\mu\nu}-\zeta\frac{k_\mu k_\nu}{k^2}, \tag{3}$$

which allows us to interpolate continuously from the projector (2) to the transversal one (with $\zeta=1$). Furthermore, we will also use the general form of the quadratically ultraviolet divergent tadpole to remove these unwanted ultraviolet divergencies.

Here we employ the conventions and notations of Ref. [1]. As usual for Dyson-Schwinger studies all integrals are formulated in Euclidean space-time. $Z(k^2)$ is the gluon renormalization function defined via the gluon propagator in Landau gauge

$$D^{ab}_{\mu\nu}(k)=\delta^{ab}\left(\delta_{\mu\nu}-\frac{k_\mu k_\nu}{k^2}\right)\frac{Z(k^2)}{k^2}. \tag{4}$$

The deviation of $Z(k^2)$ from its tree-level value $Z\equiv 1$ provides a measure for renormalization of the gluon field due to the considered interactions. The ghost renormalization function $G(k^2)$ is defined analogously via the ghost propagator, see Eq. (1).

In Landau gauge the ghost-gluon vertex does not attribute an independent ultraviolet divergence, i.e. one has $\tilde{Z}_1=1$ [26]. Therefore a truncation based on the tree-level form for the ghost-gluon vertex function, $G_\mu(q,p)=iq_\mu$ is compatible with the desired short distance behavior of the solutions. This will be exploited in the following.

To proceed we will first consider the truncation schemes of Refs. [3,4] in the next two subsections. Both these truncation schemes employ only the projector $\mathcal{R}_{\mu\nu}$ (2) in the gluon equation. The main difference between these truncation schemes consists in the treatment of the three-point functions. Whereas in Ref. [3] the form of ghost-gluon and three-gluon vertex function has been related to the gluon and ghost renormalization functions using Slavnov-Taylor identities (and then the resulting system has been solved self-consistently), in Ref. [4] bare three-point functions have been used. Amazingly, though, both schemes provide results with identical qualitative infrared behavior: the gluon propagator vanishes in the infrared, the ghost propagator is highly singluar there, and the strong running coupling (which can be related to the gluon and ghost renormalization functions using the specific form of the ghost-gluon vertex in Landau gauge [3]) has an infrared fixed point. Because this infrared behavior is determined by the interplay between the ghost loop in the gluon equation (the gluon loop being subleading in the infrared) and the ghost equation such a scenario is also found in the ghost-loop only approximation [4]. We will exploit these two recent truncation schemes in the course of this article for various tests of our method.

A. The dressed vertex truncation including the gluon loop

In Ref. [3] an approximation scheme for the longitudinal parts of ghost-gluon and 3-gluon vertex functions has been employed which ensures consistency at the level of one-particle Green's functions, i.e. propagators. The detailed form of the vertex functions can be found in Ref. [3]. Here we provide directly the ghost

$$\begin{aligned}\frac{1}{G(k^2)}=\tilde{Z}_3-g^2N_c\int\frac{d^4q}{(2\pi)^4}(k\mathcal{P}^{(1)}(p)q)\\ \times\frac{Z(p^2)G(q^2)}{k^2p^2q^2}\left(\frac{G(p^2)}{G(q^2)}+\frac{G(p^2)}{G(k^2)}-1\right),\\ p=k-q,\end{aligned} \tag{5}$$

and the gluon

$$\begin{aligned}\frac{1}{Z(k^2)}=Z_3-Z_1\frac{g^2N_c}{6}\int\frac{d^4q}{(2\pi)^4}\Bigg\{N_1(p^2,q^2;k^2)\\ \times\frac{Z(p^2)G(p^2)Z(q^2)G(q^2)}{Z(k^2)G^2(k^2)}\\ +N_2(p^2,q^2;k^2)\frac{Z(p^2)G(p^2)}{G(q^2)}\\ +N_2(q^2,p^2;k^2)\frac{Z(q^2)G(q^2)}{G(p^2)}\Bigg\}\frac{G(k^2)}{k^2p^2q^2}\\ +\frac{g^2N_c}{3}\int\frac{d^4q}{(2\pi)^4}\{(q\mathcal{R}(k)q)(G(k^2)G(p^2)\\ -G(q^2)G(p^2))-(q\mathcal{R}(k)p)G(k^2)G(q^2)\}\\ \times\frac{1}{k^2p^2q^2}\end{aligned} \tag{6}$$

equations, respectively. The functions $N_1(x,y;z)=N_1(y,x;z)$ and $N_2(x,y;z)$ are given in Appendix C of Ref. [3].

In Eq. (5) we have already exploited the identity $\tilde{Z}_1=1$. This leaves the gluon and ghost field renormalization constants Z_3 and $\tilde{Z}_3$ as well as the gluon vertex renormalization constant Z_1 to be determined correspondingly to the employed truncation. Note that these constants depend on the ultraviolet cutoff Λ and the renormalization scale μ.

In Ref. [3] different angular approximations for $q^2>k^2$ and for $q^2<k^2$ have been employed. In the latter case $G(p^2)=G((k-q)^2)\to G(k^2)$ and $Z(p^2)\to Z(k^2)$ have been set which obviously preserves the limit $q^2\to 0$ of the integrand. With this approximation one obtains from Eq. (5) upon angular integration

$$\begin{aligned}\frac{1}{G(k^2)}=\tilde{Z}_3-\frac{g^2}{16\pi^2}\frac{3N_c}{4}\Bigg\{\int_0^{k^2}\frac{dq^2}{k^2}\frac{q^2}{k^2}Z(k^2)G(k^2)\\ +\int_{k^2}^{\Lambda^2}\frac{dq^2}{q^2}Z(q^2)G(q^2)\Bigg\}\end{aligned}$$

$$= \tilde{Z}_3 - \frac{g^2}{16\pi^2}\frac{3N_c}{4}\left(\frac{1}{2}Z(k^2)G(k^2) + \int_{k^2}^{\Lambda^2}\frac{dq^2}{q^2}Z(q^2)G(q^2)\right), \tag{7}$$

where we introduced an $O(4)$-invariant momentum cutoff Λ to account for the logarithmic ultraviolet divergence, which will have to be absorbed by the renormalization constants. With some further assumptions the angular approximation for the gluon equation (6) yields

$$\frac{1}{Z(k^2)} = Z_3 + Z_1\frac{g^2}{16\pi^2}\frac{N_c}{3}\left\{\int_0^{k^2}\frac{dq^2}{k^2}\left(\frac{7}{2}\frac{q^4}{k^4} - \frac{17}{2}\frac{q^2}{k^2} - \frac{9}{8}\right) \times Z(q^2)G(q^2) + \int_{k^2}^{\Lambda^2}\frac{dq^2}{q^2}\left(\frac{7}{8}\frac{k^2}{q^2} - 7\right)Z(q^2)G(q^2)\right\} + \frac{g^2}{16\pi^2}\frac{N_c}{3}\left\{\int_0^{k^2}\frac{dq^2}{k^2}\frac{3}{2}\frac{q^2}{k^2}G(k^2)G(q^2) - \frac{1}{3}G^2(k^2) + \frac{1}{2}\int_{k^2}^{\Lambda^2}\frac{dq^2}{q^2}G^2(q^2)\right\}. \tag{8}$$

In the infrared the solutions $Z(x)$ and $G(x)$ behave powerlike:

$$Z(x) \propto x^{2\kappa}, \quad G(x) \propto x^{-\kappa}. \tag{9}$$

In this truncation scheme one obtains $\kappa \approx 0.92$ [3]. To solve the coupled system for all momenta the power laws, Eq. (9), are used to perform the integrals from $y=0$ to an infrared point $y=\epsilon$ analytically, while the remaining part of the integrals is done with the help of numerical routines, see e.g. Ref. [25].

The nonperturbative subtraction scheme of Ref. [3] implies a strong running coupling with infrared fixed point. Starting again from the nonrenormalization of the ghost-gluon vertex

$$\tilde{Z}_1 = Z_g Z_3^{1/2}\tilde{Z}_3 = 1, \tag{10}$$

one can readily show that the product $g^2 Z(\mu^2)G^2(\mu^2)$ is renormalization group invariant. Therefore, in the absence of any dimensionful parameter, this (dimensionless) product is a function of the running coupling $\bar{g}$ only. Analyzing this renormalization group invariant product more closely one concludes that it is identical to the running coupling $\bar{g}^2(\mu^2)$. As the infrared powers in the product ZG^2 cancel exactly the running coupling is a finite constant for $\mu^2=0$.

B. The bare vertex ghost-loop only truncation

Substituting the tree-level ghost-gluon vertex for the dressed one and neglecting the gluon loop the coupled system of equations (5),(6) reads

$$\frac{1}{G(k^2)} = \tilde{Z}_3 - g^2 N_c \tilde{Z}_1 \int \frac{d^4q}{(2\pi)^4}\frac{k^2q^2-(k\cdot q)^2}{k^2q^2(k-q)^4}G(q^2)Z((k-q)^2), \tag{11}$$

$$\frac{1}{Z(k^2)} = Z_3 + g^2\frac{N_c}{3}\tilde{Z}_1 \int \frac{d^4q}{(2\pi)^4}\frac{k^2(k^2+q^2+(k-q)^2)+4q^2(k-q)^2-2(k-q)^4-2q^4}{2k^4q^2(k-q)^2}G(q^2)G((k-q)^2). \tag{12}$$

To simplify notation we introduce the abbreviations $x := k^2$, $y := q^2$, $s := \mu^2$ and $L := \Lambda^2$. In the angular approximation of Ref. [4] ("ymax approximation") where $Z(\min(p^2,q^2))$ and $G(\min(p^2,q^2))$ are substituted for $Z((k-q)^2)$ and $G((k-q)^2)$ Eqs. (11),(12) are simplified to

$$\frac{1}{G(x)} = \tilde{Z}_3(s,L) - \frac{9}{4}\frac{g^2N_c}{48\pi^2}\left(Z(x)\int_0^x\frac{dy}{x}\frac{y}{x}G(y) + \int_x^L\frac{dy}{y}Z(y)G(y)\right), \tag{13}$$

$$\frac{1}{Z(x)} = Z_3(s,L) + \frac{g^2N_c}{48\pi^2}\left(G(x)\int_0^x\frac{dy}{x}\left(-\frac{y^2}{x^2}+\frac{3y}{2x}\right) \times G(y) + \int_x^L\frac{dy}{2y}G^2(y)\right). \tag{14}$$

Imposing as renormalization conditions $Z(s)=G(s)=1$ to determine Z_3 and $\tilde{Z}_3$ these equations may be solved numerically for a given [O(4) invariant] cutoff. As a matter of fact, we use subtracted finite equations in our numerical procedure; see Appendix C for details.

In the infrared, also the solutions of Eqs. (13),(14) behave powerlike, cf. Eq. (9), with $\kappa \approx 0.77$ [4]. In the same truncation but with no angle approximation employed a solution $\kappa=1$ has been extracted for the infrared behavior. However, it will be explained below that we could not find a numerical solution for nonvanishing momenta connected to the $\kappa=1$ infrared behavior.

C. The bare vertex truncation including the gluon loop

In this subsection we will detail a novel truncation scheme which employs bare vertices. Nevertheless it will be constructed such that it reproduces the correct perturbative limit for large momenta. To analyze the gluon loop we will use the class of projectors $\mathcal{P}^{(\zeta)}_{\mu\nu}$ (3). A smooth interpolation

between the Brown-Pennington projector ($\zeta=4$) and the transverse one ($\zeta=1$) will be helpful in the analysis of unphysical quadratic ultraviolet divergencies for $\zeta\neq 4$ in the gluon equation. Their careful removal is essential for a numerical solution retaining the infrared behavior of the solutions.

The coupled equations for the ghost and gluon dressing functions using bare vertices read as follows [the ghost equation is, of course, identical to Eq. (11); it is only repeated for a coherent representation]:

$$\frac{1}{G(x)}=\tilde{Z}_3-g^2N_c\int\frac{d^4q}{(2\pi)^4}\frac{K(x,y,z)}{xy}G(y)Z(z), \quad (15)$$

$$\frac{1}{Z(x)}=Z_3+g^2\frac{N_c}{3}\int\frac{d^4q}{(2\pi)^4}\frac{M(x,y,z)}{xy}G(y)G(z) + Z_1g^2\frac{N_c}{3}\int\frac{d^4q}{(2\pi)^4}\frac{Q(x,y,z)}{xy}Z(y)Z(z). \quad (16)$$

The kernels ordered with respect to powers of $z:=p^2=(k-q)^2$ have the form

$$K(x,y,z)=\frac{1}{z^2}\left(-\frac{(x-y)^2}{4}\right)+\frac{1}{z}\left(\frac{x+y}{2}\right)-\frac{1}{4} \quad (17)$$

$$M(x,y,z)=\frac{1}{z}\left(\frac{\zeta-2}{4}x+\frac{y}{2}-\frac{\zeta}{4}\frac{y^2}{x}\right)+\frac{1}{2}+\frac{\zeta}{2}\frac{y}{x}-\frac{\zeta}{4}\frac{z}{x} \quad (18)$$

$$Q(x,y,z)=\frac{1}{z^2}\left(\frac{1}{8}\frac{x^3}{y}+x^2-\frac{19-\zeta}{8}xy+\frac{5-\zeta}{4}y^2+\frac{\zeta}{8}\frac{y^3}{x}\right) + \frac{1}{z}\left(\frac{x^2}{y}-\frac{15+\zeta}{4}x-\frac{17-\zeta}{4}y+\zeta\frac{y^2}{x}\right) - \left(\frac{19-\zeta}{8}\frac{x}{y}+\frac{17-\zeta}{4}+\frac{9\zeta}{4}\frac{y}{x}\right) + z\left(\frac{\zeta}{x}+\frac{5-\zeta}{4y}\right)+z^2\frac{\zeta}{8xy}. \quad (19)$$

It is straightforward to verify that for $\zeta=4$ the kernel $M(x,y,z)$ is identical to the kernel in Eq. (12).

The quadratic ultraviolet divergencies of the integrals are most easily discovered approximating the angular integrals as done in the previous subsections (note that we will use these approximations only for an analysis of the ultraviolet behavior) and introducing an Euclidean sharp cutoff. Displaying only the ultraviolet divergent integrals

$$\frac{g^2N_c}{48\pi^2}\int_x^L\frac{dy}{x}\left(\left(\frac{4-\zeta}{4}+\frac{\zeta-2}{4}\frac{x}{y}\right)G^2(y) + Z_1\left(\frac{3\zeta-12}{2}-\frac{\zeta+24}{4}\frac{x}{y}+\frac{7}{8}\frac{x^2}{y^2}\right)Z^2(y)\right) \quad (20)$$

one sees that for $\zeta=4$ the terms independent of the integration momentum y vanish. Thus these integrals are then only logarithmically ultraviolet divergent as could be expected on the basis of the results summarized in the previous subsections. Of course, the quadratic ultraviolet divergencies are artifacts of the employed truncation. Due to gauge invariance they would cancel against the tadpole and similar divergencies in the two-loop terms. The calculation of the latter being beyond the scope of this paper we will simply subtract these divergent terms. This cannot be done straightforwardly at the level of integrands: Such a procedure would disturb the infrared properties of the Dyson-Schwinger equations. As we anticipate from previous studies and analytic work [6,7] that the ghost loop is the leading contribution in the infrared the natural place to subtract the quadratically ultraviolet divergent constant is the gluon loop. We do this by employing the substitution

$$Q(x,y,z)\to Q'(x,y,z)=Q(x,y,z)+\tfrac{5}{4}(4-\zeta) \quad (21)$$

in Eq. (16). At first sight, due to the presence of the prefactor Z_1 in the gluon loop, this seems not to be sufficient to remove also the quadratic ultraviolet divergence of this ghost loop. However, note that in the next step we will enforce consistency of the logarithmic divergencies which entails then cancelation of the quadratic divergencies if Q' is employed in the gluon loop; see below.

To achieve the correct one-loop scaling in the ultraviolet we will adopt a similar treatment to the one of Ref. [3]. Please note that within the presented class of truncation schemes it is impossible to satisfy both correct one-loop scaling and the Slavnov-Taylor identity $Z_1=Z_3/\tilde{Z}_3$. For large Euclidean momenta and to one loop the behavior of the propagator functions can be described as

$$Z(x)=Z(s)\left[\omega\log\left(\frac{x}{s}\right)+1\right]^{\gamma}, \quad (22)$$

$$G(x)=G(s)\left[\omega\log\left(\frac{x}{s}\right)+1\right]^{\delta}. \quad (23)$$

$Z(s)$ and $G(s)$ denote the value of the dressing functions at some renormalization point $s:=\mu^2$; γ and δ are the respective anomalous dimensions. To one loop one has $\delta=-9/44$ and $\gamma=-1-2\delta$ for arbitrary number of colors N_c and no quarks, $N_f=0$ [27]. Furthermore, $\omega=11N_c\alpha(s)/12\pi$.

Employing these expressions in the ghost equation (15) and approximating the angular integrals as done previously one obtains to the order of the leading logarithms

$$G^{-1}(s)\left[\omega\log\left(\frac{x}{s}\right)+1\right]^{-\delta}=\tilde{Z}_3-\frac{9g^2Z(s)G(s)}{64\pi^2\omega(\gamma+\delta+1)} \times\left\{\left[\omega\log\left(\frac{L}{s}\right)+1\right]^{\gamma+\delta+1} -\left[\omega\log\left(\frac{x}{s}\right)+1\right]^{\gamma+\delta+1}\right\} \quad (24)$$

where the abbreviation $L:=\Lambda^2$ has been used again. The renormalization constant $\tilde{Z}_3(L,s)$ cancels the cutoff dependence of the first term in the bracket. Thus, the power and the prefactor of the second term have to match with the left-hand side of this equation. This leads to two conditions:

$$\gamma+2\delta+1=0, \tag{25}$$

$$\frac{9}{2\omega(\gamma+1)}\frac{g^2}{16\pi^2}Z(s)G^2(s)=1. \tag{26}$$

Equation (25) is of course nothing else but consistency of the ghost equation with one-loop scaling.

Plugging the ultraviolet behavior (22) and (23) into the gluon equation (16) and keeping the leading order logarithms leads to

$$\begin{aligned} Z^{-1}(s)&\left[\omega\log\left(\frac{x}{s}\right)+1\right]^{-\gamma} \\ &=Z_3-\frac{g^2G^2(s)}{32\pi^2\omega\gamma}\left\{\left[\omega\log\left(\frac{L}{s}\right)+1\right]^{-\gamma}\right. \\ &\quad\left.-\left[\omega\log\left(\frac{x}{s}\right)+1\right]^{-\gamma}\right\}-\frac{7g^2Z(s)G(s)}{16\pi^2} \\ &\quad\times\int_x^L dyZ_1\left[\omega\log\left(\frac{y}{s}\right)+1\right]^{\gamma+\delta}. \end{aligned} \tag{27}$$

Here we see that due to the employed truncation we have to give up either one-loop scaling or the Slavnov-Taylor identity $Z_1=Z_3/\tilde{Z}_3$. Note, however, that $Z_3(L,s)$ has the correct cutoff dependence to make this equation finite with finite $Z_1(L,s)$. Nevertheless, in order to get the correct leading log contribution from the gluon loop the integrand in the last line should be proportional to $[\omega\log(y/s)+1]^{-\gamma-1}$. This not only contradicts the identity $Z_1=Z_3/\tilde{Z}_3$ but also requires the renormalization *constant* $Z_1(L,s)$ to acquire a momentum dependence if correct one-loop scaling is to be enforced. Following case (c) described in Chap. 6 of Ref. [3] we demand therefore

$$\begin{aligned} Z_1(L,s)&\to\mathcal{Z}_1(x,y,z;s,L) \\ &\sim\left[\omega\log\left(\frac{y}{s}\right)+1\right]^{-\delta-2\gamma-1}. \end{aligned} \tag{28}$$

Generalizing the approach of Ref. [3] we note that the following two-parameter ansatz:

$$\mathcal{Z}_1(x,y,z;s,L)=\frac{G(y)^{(1-a/\delta-2a)}}{Z(y)^{(1+a)}}\frac{G(z)^{(1-b/\delta-2b)}}{Z(z)^{(1+b)}} \tag{29}$$

with arbitrary a and b satisfies the required proportionality. This can be straightforwardly verified with the help of expression (25) obtained from the ghost equation. In addition ansatz (29) ensures the cancelation of quadratic ultraviolet divergencies as discussed above also if $\zeta\neq4$.

Carrying out the remaining integral in Eq. (27) and matching powers one obtains

$$\gamma+2\delta+1=0, \tag{30}$$

$$\begin{aligned} &\frac{1}{2\gamma\omega}\frac{g^2}{16\pi^2}Z(s)G^2(s) \\ &\quad-\frac{7}{\gamma\omega}\frac{g^2}{16\pi^2}Z(s)^{1-a-b}G(s)^{2-a/\delta-b/\delta-2a-2b}=1. \end{aligned} \tag{31}$$

First of all, we reproduce correct one-loop scaling also from the gluon equation as can be seen from the equivalence of Eqs. (30) and (25). Second, with the perturbative renormalization conditions $Z(s)=G(s)=1$ which are possible and appropriate at a large Euclidean renormalization point μ one obtains together with Eq. (26) the correct anomalous dimensions $\gamma=-13/22$ and $\delta=-9/44$.

A reasonable choice of parameters is of course one which keeps $\mathcal{Z}_1$ as weakly dependent as possible on the momenta y and z, cf. Fig. 10 in Appendix A. Note that the choice $a=b=0$ corresponds to the truncation scheme of [28] whereas $a=3\delta, b=0$ together with the appropriate vertex dressings reproduces case (c) of Ref. [3]. The infrared behavior of the gluon loop in the gluon equation depends strongly on a and b. E.g. for $b=0$ one can distinguish three cases: For $a<0$ the gluon loop is subleading in the infrared; for $a=0$ as in Ref. [28] the gluon loop produces the same power as the ghost loop; for $a>0$ the gluon loop becomes the leading term in the infrared. In the last case we did not find a solution to the coupled gluon-ghost system. In Appendix A we will demonstrate that $a=b=3\delta$ minimizes the momentum dependence of $\mathcal{Z}_1$. Thus we will use these values, unless stated otherwise, explicitly.

The infrared behavior of the propagator functions in this truncation scheme and for the transverse projector ($\zeta=1$) has been determined very recently [6,7]. It can be shown straightforwardly that the relation between ghost and gluon infrared behavior is again as in Eq. (9). This is expected also on general grounds [5]. Due to this one can immediately use the *Ansätze*

$$Z(x)\to Ax^{2\kappa},\quad G(x)\to Bx^{-\kappa}\quad\text{for}\quad x\to0. \tag{32}$$

As is explained in detail in Ref. [7] the renormalization constants Z_3 and $\tilde{Z}_3$ can be dropped for very small momenta x: They are either subleading in the infrared (gluon equation) or have to be zero when the renormalization takes place at $\mu=0$ (ghost equation). The remaining infrared integrals can be evaluated using the formula [7]

$$\int d^4qy^az^b=\pi^2x^{2+a+b}\frac{\Gamma(2+a)\Gamma(2+b)\Gamma(-a-b-2)}{\Gamma(-a)\Gamma(-b)\Gamma(4+a+b)}, \tag{33}$$

where again $x=k^2$, $y=q^2$ and $z=(k-q)^2$. From the resulting two conditions

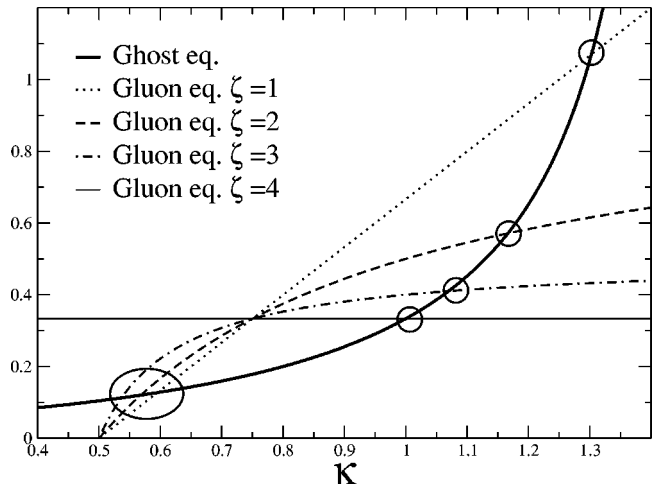

FIG. 3. Here the graphical solution to Eqs. (34) and (35) is shown. The thick line represents the left hand side of Eq. (34), whereas the other four curves depict the left hand side of Eq. (35) for different values of the parameter ζ. The ellipse marks the bulk of solutions between $\kappa=0.5$ and $\kappa=0.6$ for different ζ, whereas the circles show the movement of the solution $\kappa=1.3$ for a transverse projector to $\kappa=1$ for the Brown-Pennington case, $\zeta=4$.

$$\frac{1}{18}\frac{(2+\kappa)(1+\kappa)}{(3-2\kappa)}=\frac{\Gamma^2(2-\kappa)\Gamma(2\kappa)}{\Gamma(4-2\kappa)\Gamma^2(1+\kappa)}\frac{g^2N_c}{48\pi^2}AB^2, \tag{34}$$

$$\frac{4\kappa-2}{4\zeta\kappa-4\kappa+6-3\zeta}=\frac{\Gamma^2(2-\kappa)\Gamma(2\kappa)}{\Gamma(4-2\kappa)\Gamma^2(1+\kappa)}\frac{g^2N_c}{48\pi^2}AB^2, \tag{35}$$

one obtains the determining relation for κ by equating both left hand sides; see Fig. 3. For the Brown-Pennington projector, i.e. $\zeta=4$, one then finds the known solution $\kappa=1$ [4]. However, as can be seen immediately the left-hand side of the second equation possesses a zero for $\kappa=1/2$ which is canceled by a pole only for $\zeta=4$. Lowering ζ only slightly a further solution with κ slightly larger than 0.5 exists. For the transverse projector, i.e. $\zeta=1$, this latter solution becomes $\kappa=0.59\ldots$ in accordance with Refs. [6,7]. Also the solution $\kappa=1$ changes continuously when lowering ζ. The corresponding κ are then all larger than 1 and contradict the masslessness condition; see Chap. 5 of Ref. [1] for a discussion of this condition. The main result of this paper is that the infrared behavior $\kappa\approx0.5$ matches to a numerical solution whereas no numerical solution could be found with the infrared behavior $\kappa=1$.

The renormalization group analysis for the running coupling given in Ref. [3] certainly applies here as well. The renormalization group invariant expression for the running coupling is therefore given by

$$\alpha(x)=\frac{g^2}{4\pi}Z(x)G^2(x). \tag{36}$$

As can be seen directly from Eqs. (34),(35), in the here presented truncations the product $N_cg^2AB^2$ is constant for a given κ. With $\alpha(0)=g^2AB^2/4\pi$ one concludes immediately that $\alpha(x)$ is proportional to N_c^{-1}. Furthermore, the ghost and gluon dressing functions $Z(x)$ and $G(x)$ are independent of the number of colors: N_c enters the Dyson-Schwinger equations only in the combination g^2N_c at our level of truncation. From the solution $\kappa=0.5953$ of the infrared analysis with the transverse projector $\zeta=1$ one determines the infrared fixed point of the running coupling to be $\alpha(0)=2.972$ for $N_c=3$.

III. GLUON AND GHOST DYSON-SCHWINGER EQUATIONS ON A FOUR-TORUS

There are three central aims connected to the investigation of the Dyson-Schwinger equations on a four-torus. The first one is purely technical: This allows us to study finite volume effects also in the Dyson-Schwinger approach. Monte Carlo simulations on a lattice necessarily have to be done in a finite volume. Therefore in the latter kind of approach infrared properties are only accessible by extrapolations to an infinite volume where the available data are gained on several different volumes which, due to limitations in computer time, do only differ at best by one order of magnitude. We will see in the present Dyson-Schwinger approach that available volumes cover several orders of magnitude. And more importantly, in several truncations and approximations one can compare to the results obtained in an infinite volume.

The second issue is the solution of the (truncated) Dyson-Schwinger equations without any angular approximations. We will detail below why and how this can be achieved on the momentum grid dual to the four-torus. This will also lead us to the main result of this paper discussed in the following section.

The third aim relates to the possibility of topological obstructions on a compact manifold. It is well known e.g. that a four-torus allows for a nonvanishing Pontryagin index. We hope that we will be able to describe the solutions of Dyson-Schwinger equations with twisted boundary conditions [29] in a subsequent publication. And choosing an asymmetric four-torus might allow the introduction of a nonvanishing temperature in a relatively simple way.

A. Finite volume effects

From a technical point of view using as an underlying manifold a four-torus or choosing periodic boundary conditions on a hypercube is identical. Note that the definition of the Faddeev-Popov operator necessitates periodic boundary conditions for ghosts instead of their Grassmannian nature, see e.g. Ref. [30]. With L being the length in every direction of the hypercube the four-dimensional momentum integral has to be substituted by a sum over four indices,

$$\int\frac{d^4q}{(2\pi)^4}\to\frac{1}{L^4}\sum_{j_1,j_2,j_3,j_4}. \tag{37}$$

On the other hand, the quantities of interest, the gluon and ghost renormalization function, $Z(k^2)$ and $G(k^2)$, respectively, do only depend on the O(4) invariant squared momenta as long as all directions are treated on an equal footing

on the torus. This suggests relabeling the points on the momentum grid not according to a Cartesian but a hypersherical coordinate system,

$$\frac{1}{L^4}\sum_{j_1,j_2,j_3,j_4} = \frac{1}{L^4}\sum_{j,l}\ , \tag{38}$$

where the index j numbers the hyperspheres $q^2=\text{const}$. The index l, which numbers the grid points on each hypersphere respectively, will be dropped in the following.

In the integrals to be discretized there appear three momenta: the external momentum, labeled k, the loop momentum q and for the second propagator in the loop $p=k-q$. We will use the following notation:

$$\begin{aligned} x &:= k^2 \quad \text{with} \quad x_i \in \text{hypersphere}\, i, \\ y &:= q^2 \quad \text{with} \quad y_j \in \text{hypersphere}\, j, \\ z &:= p^2 = (k-q)^2 \quad \text{with} \quad z_n \in \text{hypersphere}\, n. \end{aligned} \tag{39}$$

On the hypercubic momentum grid dual to the four-torus the momentum $p=k-q$ is located on the grid for every pair of grid momenta k and q as can be seen from elementary vector operations (or from the analogue of cubic lattices in solid state physics).

Note that we have introduced an O(4) invariant cutoff Λ into Eqs. (7),(8). As we will see below in more detail a corresponding regularization of the sums over grid momenta is required. In a first step we set up a momentum grid with $j_1,j_2,j_3,j_4=-N,\ldots,0,\ldots N$. The hypercube property of this lattice seems to suggest in the first place to cut off the sums such that overcomplete hypercubes are summed. Such a method, however, breaks O(4) invariance and introduces sizeable numerical errors. [Note that in lattice Monte Carlo simulations the analysis of the resulting data for O(4) invariance necessitates special kinds of cuts through the lattice [9].] As can be seen from Fig. 4 an O(4) invariant cutoff of the sums necessitates neglecting the ''edges:'' The sum extends only over the fully drawn hypersheres, and we omit the summation over the dashed ones.

To be able to compare to already known flat space solutions we will first solve the torus analogue of the equations with angle approximations, i.e. Eqs. (7),(8) or Eqs. (13),(14). To this end we start from Eqs. (5),(6) or Eqs. (11),(12), respectively. After formulating the corresponding four-dimensional integrals as sums over lattice momenta the functional dependence of the propagator functions is approximated according to the rules described in Secs. II A and II B, respectively. We give the explicit expressions for the bare vertex ghost-loop only truncation. The corresponding ones for dressed vertex truncation can be derived analogously in a straightforward manner; however, as these are quite lengthy we do not give their explicit form.

The Dyson-Schwinger equations in bare vertex ghost-loop only truncation with angle approximation read, on the torus,

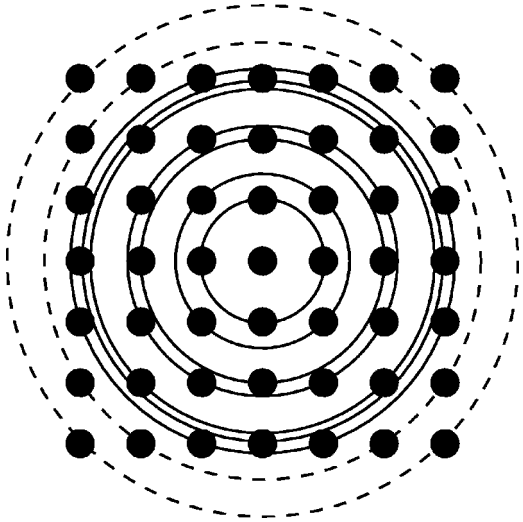

FIG. 4. Sketch of the momentum grid dual to the four-torus and the summation over complete hyperspheres indicated by fully drawn circles. The hyperspheres depicted by dashed lines are not complete due to the numerical ultraviolet cutoff.

$$\frac{1}{G(x_i)} = \tilde{Z}_3(s,L) - g^2 N_c \frac{1}{L^4}\sum_j \frac{K(x_i,y_j,z_n)}{x_i y_j} \times G(y_j) Z(\max(x_i,y_j)), \tag{40}$$

$$\frac{1}{Z(x_i)} = Z_3(s,L) + g^2 \frac{N_c}{3}\frac{1}{L^4}\sum_j \frac{M(x_i,y_j,z_n)}{x_i y_j} \times G(y_j) G(\max(x_i,y_j)). \tag{41}$$

As shown in the previous subsection the momentum $p=k-q$ which satisfies $z_n=(k-q)^2$ lies on the momentum grid, and furthermore, $p=k-q$ is determined uniquely from k and q for which $x_i=k^2$ and $y_j=q^2$ by using elementary vector operations. Note, however, that $\sqrt{p^2}$ might be larger than the ultraviolet cutoff even if $\sqrt{k^2}$ and $\sqrt{q^2}$ are not. The actual treatment of the sums in Eqs. (40),(41) can nevertheless be done straightforwardly as the exact algebraic expressions for the kernels are known.

The main difference between the equations on the torus and the flat space equations is the effective treatment in the infrared. The finite volume in coordinate space leads to a finite value of squared momentum for the first hypersphere $j=1$. Thus one has not to worry about possible infrared singularities. On the other hand, there exists zero modes on the four-torus. In all the calculations presented here they are neglected; an estimate of their possible contribution is given in Appendix B. Note furthermore that for the numerical solution as described in Refs. [3,25] the disadvantage of dealing with infrared singularities has been turned into a benefit: The infrared behavior of the propagator functions has been determined via an asymptotic series calculating the corresponding coefficients and powers analytically. Matching these series at some finite momentum to the functions as obtained from standard numerical techniques finally enabled us to numerically solve the coupled integral equations. Such a compli-

cated process is not necessary employing a torus. However, one anticipates already at this level some deviations in the infrared between the solutions obtained in these different ways. In the next section the corresponding numerical results will be discussed. They demonstrate that using a torus as infrared cutoff works surprisingly well.

B. Dyson-Schwinger equations with angle integrals on the torus

The intricacy of the infrared analysis has prevented so far a solution of the coupled gluon-ghost system without angular approximations. Using a torus as an infrared regulator opens up the possiblity to solve these equations directly without any recourse to an infrared asymptotic expansion. As recent arguments have been provided that the use of a bare ghost-gluon vertex is not inferior to employing a dressed one [6,7] we will solve the system in the truncation described in Sec. II C.

With the above discussed replacement of $\int[d^4q/(2\pi)^4] \rightarrow (1/L^4)\Sigma_j$ Eqs. (15),(16) read on the torus

$$\frac{1}{G(x_i)} = \tilde{Z}_3(s,L) - g^2 N_c \frac{1}{L^4} \sum_j \frac{K(x_i,y_j,z_n)}{x_i y_j} \times G(y_j) Z(z_n), \tag{42}$$

$$\frac{1}{Z(x_i)} = Z_3(s,L) + g^2 \frac{N_c}{3} \frac{1}{L^4} \sum_j \frac{M(x_i,y_j,z_n)}{x_i y_j} \times G(y_j) G(z_n) + g^2 \frac{N_c}{3} \frac{1}{L^4} \sum_j \frac{Q'(x_i,y_j,z_n)}{x_i y_j} \times G^{1-a/\delta-2a}(y_j) G^{1-b/\delta-2b}(z_n) \times Z^{-a}(y_j) Z^{-b}(z_n). \tag{43}$$

As already stated $\sqrt{z}$ might be larger than the ultraviolet cutoff even if $\sqrt{x}$ and $\sqrt{y}$ are not. Again the kernels can be nevertheless evaluated straightforwardly, however, if z with $L<z<4L$ is the argument of a propagator function we set $z=L$, i.e. we approximate $Z(z)$ or $G(z)$ then by $Z(L)$ or $G(L)$, respectively. Another more elaborate treatment consists of matching the corresponding perturbative ultraviolet tail to the function under consideration. This has been applied in some cases to test the viability of the method.

IV. NUMERICAL RESULTS

A. Comparing torus solutions to previous results in flat space-time

The solutions of the Dyson-Schwinger equations on the torus can be compared in two different ways to the ones obtained in flat space-time. First, one can use the solutions of the ''continuum'' equations for a certain cutoff Λ and certain renormalization scale μ to provide the values for $Z_3(\mu^2,\Lambda^2)$ and $\tilde{Z}_3(\mu^2,\Lambda^2)$ as input for the equations on the torus which are then solved, cf. the discussion in Appendix C where the numerical methods employed to obtain the solutions of the ''continuum'' equations are summarized. Second, one can subtract both equations at the squared momenta s_G and s_Z and therefore trade the two renormalization constants for the values of the dressing functions at these momenta, namely $Z(s_Z)$ and $G(s_G)$. For the sake of comparison one can read these values from the continuum solution to be used in the torus equations. If s_Z and s_G are taken to be sufficently far in the ultraviolet region of momentum, where finite volume effects play a minor role, the two procedures lead to the same results. We have verified that this is indeed the case within the limits of numerical accuracy.

Our results for the ghost dressing function, the gluon dressing function and the running coupling in the bare-vertex ghost-only and the dressed vertex truncation can be seen in Figs. 5 and 6, respectively. In both truncation schemes we solved for three different momentum spacings corresponding to different volumes in coordinate space. To keep the cutoff identical for all the spacings within each truncation scheme we have chosen three different grid sizes respectively. For the bare vertex truncation they are $N=17^4,31^4,51^4$ and for the dressed vertex truncation they are $N=21^4,41^4,61^4$.

A physical momentum scale cannot be determined in truncation schemes which do not provide the correct perturbative running of the coupling in the ultraviolet. With the missing gluon loop this is the case in the bare vertex only truncation scheme. We therefore have to stick to an internal momentum scale without physical units in this case. The situation is different, however, in the dressed vertex truncation scheme. Here we have fixed the momentum scale by calculating the running coupling for the color group SU(3) and using the experimental value $\alpha(x)=0.118$ at $x=M_Z^2=(91.187\ \mathrm{GeV})^2$ to fix a physical scale.

In the bare vertex truncation scheme we have chosen $Z(\mu^2)=G(\mu^2)=1$ as renormalization condition where we have taken $\mu^2=\Lambda^2$, the (squared) ultraviolet cutoff. Of course, this choice is by no means special and one is completely free to choose the renormalization point wherever one likes. For the numerical calculation in flat space we have chosen two different subtraction points for the ghost and the gluon equations as described in Appendix C. For good convergence of the iteration process the ghost equation is most conveniently subtracted at zero momentum, whereas the gluon equation can be subtracted at any value of squared momentum in the region where the equations are solved numerically. In our calculation we chose the cutoff $\Lambda^2=0.2$ in internal units as a subtraction point for the gluon equation. This allows us to use the renormalization condition $Z(\Lambda^2)=1$ directly as input in the calculation. The second input is provided by the coefficient A of the leading order infrared expansion of the gluon dressing function, $Z_{IR}(x)=Ax^{2\kappa}$. The condition $G(\Lambda^2)=1$ then leads to $A=357.33$. The value of the coupling at the renormalization point, $\alpha(\mu^2)$, is taken to be 0.97. Again one is completely free to choose this number arbitrarily up to the maximum value of the running coupling which is reached in the very infrared. For the torus calculations the unsubtracted equations have been used. The same coupling $\alpha(\mu^2)=0.97$ has been taken and instead of $Z(\Lambda^2)$ and A the values $Z_3(\mu^2=0.2,\Lambda^2=0.2)=0.9591$ and $\tilde{Z}_3(\mu^2$

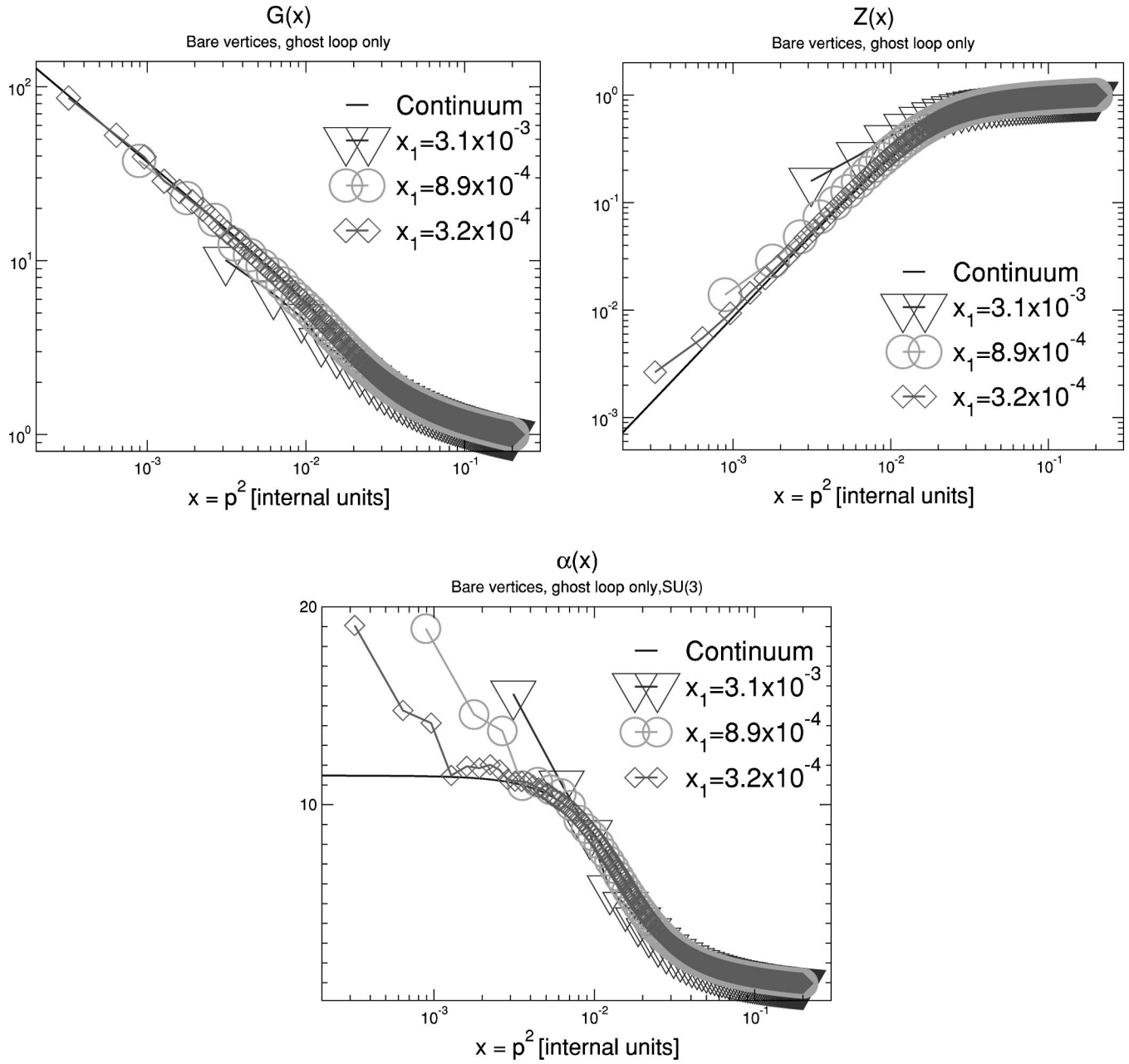

FIG. 5. Shown are the ghost dressing function, the gluon dressing function and the running coupling in the bare-vertex ghost-only truncation for different momentum grid spacings corresponding to different finite volumes of the torus. The fully drawn lines labeled ''continuum'' represent the respective results for flat Euclidean space-time, i.e. continuous momenta.

$=0.2,\Lambda^2=0.2)=1.1034$ for the renormalization constants determined from the ''continuum'' solution have been employed.

As has already been mentioned, in the dressed vertex truncation scheme we determine a ''physical'' momentum scale according to experimental results. In the numerical treatment again the ghost equation has been subtracted at zero momentum whereas the gluon equation is subtracted at finite momentum. We solved both equations similar to the method described in Ref. [25], especially we introduced also the auxiliary functions $F(x)$ and $R(x)$ as defined in Ref. [3]. As input values serve the infrared expansion of $R(x)$, $R(x)=x^{\kappa}+\cdots$, and the value $R(s)=0.8$ at the gluon subtraction point $s=1.048$ GeV^2. For the calculations on the torus we use the unsubtracted equations with the values $Z_3(\mu^2=M_Z^2,\Lambda^2=1.255$ GeV$^2)=1.266$ and $\tilde{Z}_3(\mu^2=M_Z^2,\Lambda^2=1.255$ GeV$^2)=0.966$ for the renormalization constants which have been determined from the ''continuum'' solution.

Our numerical results, depicted in Figs. 5 and 6, show similar properties for both truncation schemes. Compared with the respective ''continuum'' solutions the ones obtained on a torus show deviations for the first few lattice points in the infrared. For higher momenta all functions on the torus approach the continuum ones. Deviations are only visible there for the curves with the largest spacings. The biggest effect can be seen for the running coupling α, which is the

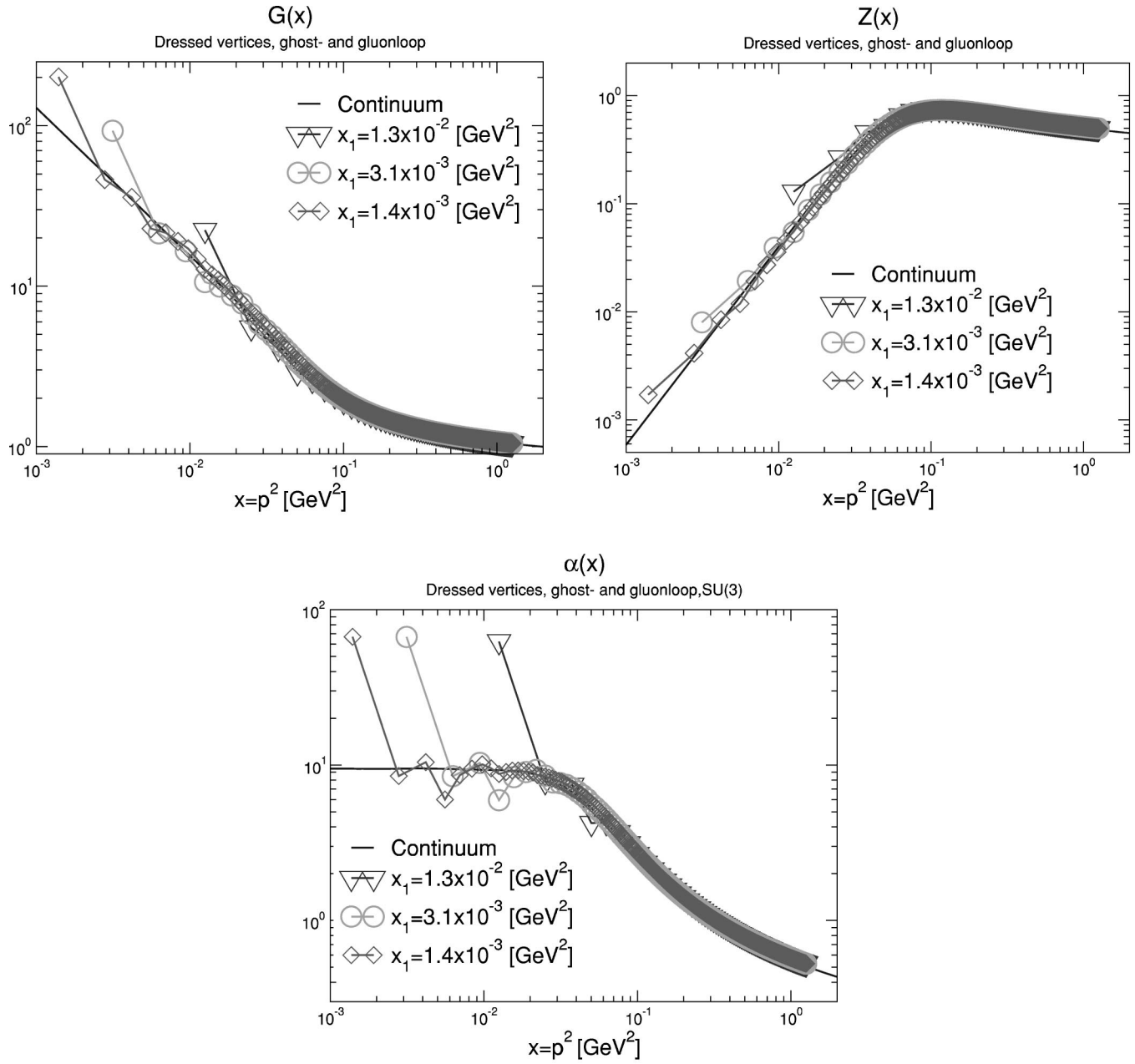

FIG. 6. The same as Fig. 5 for the dressed vertex truncation.

''observable'' of the system. As α is proportional to the product $Z(x)G^2(x)$ the deviations of the dressing functions from the ''continuum'' curve amplify in the infrared in a somewhat erratic way, so that the points in the very infrared cannot be connected by a smooth line. Comparing larger and smaller spacings of momentum grids one clearly sees that the effect is always one of the first spheres on the respective lattices and therefore moves to the infrared for smaller spacings.

The most important properties of the solutions in flat space can still be found in the torus solutions despite some deviations in the infrared. Going from larger to smaller spacings a powerlike behavior of the dressing functions in the infrared with the correct exponents can still be inferred. For the truncation scheme with dressed vertices the gluon dressing function on the torus has the same shape and the same height of the bump in the bending region of the curve. As all curves with sufficently small momentum spacing follow the correct power behavior within numerical errors we conclude that one surely can address the question of the value of the power κ in the infrared on a manifold with finite volume as has been used here or as one uses in lattice calculations. This is the central result of the present section: Employing a torus as infrared regularization is possible. In the following section we will use this to go beyond the angular approximation.

B. Numerical solutions without angular approximations

In this section we discuss our numerical results for the bare vertex truncation scheme with various projectors in the

gluon equation. We show results for the gluon and ghost dressing function and the running coupling calculated on a torus without any angular approximations. Note that up to now in the gluon-ghost Dyson-Schwinger equations solutions for nonvanishing momenta have been obtained only employing some sort of angular approximation. Going beyond these approximations we will use our new truncation scheme introduced in Sec. II C. The reason for this is that the dressed vertex truncation scheme is quite complicated, and in its derivation one has dismissed terms which seem to be crucial for the infrared behavior beyond the angle approximation. As the survey of gluon and ghosts infrared behaviors related to different *Ansätze* for vertex functions [7] does not provide any evidence for crucial differences between bare and dressed vertex functions the use of the latter seems to be an unnecessary complication. In the case of the bare-vertex ghost-loop only truncation with the Brown-Pennington projector no solutions for finite momenta without angular approximation have been reported yet. In fact the results presented in this section suggest that these solutions might not exist.

This time the values for the renormalization constants Z_3 and $\tilde{Z}_3$ cannot be taken from a ''continuum'' solution. Thus we use the subtracted equations on the torus in the course of the numerical solution by iteration. Both equations are subtracted at the renormalization point $\mu^2=1.9\ \mathrm{GeV}^2$. Similar to the case of the dressed vertex truncation from the last section the ''physical'' units are gained from experimental input: $\alpha(x)=0.118$ at $x=M_Z^2=(91.187\ \mathrm{GeV})^2$. The input values for the dressing functions at the renormalization point are $Z(\mu^2)=0.83$. Requiring $G(\mu^2)=1/\sqrt{Z(\mu^2)}$ then fixes the overall scale for $G(x)$. For the value of the coupling at the renormalization point we chose again $\alpha(\mu^2)=0.97$ similar to the two truncation schemes in the last section. For the presented solution on three different volumes lattice sizes of $N=13^4,43^4,71^4$ have been used.

As mentioned in the last section we did check cutoff effects by extrapolating the propagator functions at $z>\Lambda^2$ with a logarithmic tail with the correct anomalous dimensions. The results as compared to the ones obtained by simply setting $Z(z)=Z(\Lambda^2)$ and $G(z)=G(\Lambda^2)$ for all $z>\Lambda^2$ did change by less than 10^{-3}.

Our results for the dressing functions obtained with a transverse projector as shown in Fig. 7 are in agreement with the expected power behavior. The infrared critical exponent as calculated in Refs. [6,7], $\kappa=0.5953$, thus has been verified: A corresponding (numerical) solution for nonvanishing momenta exists. The gluon dressing function is remarkably stable against changes of the volume and approaches more and more the expected power solution for small momenta. For the ghost dressing function one observes again deviations of the first points in the infrared: An extraction of the correct infrared critical exponent from the numerical solution for the ghost function is hardly possible. Only some points come close to the analytical value of the continuum before the curve starts bending down again in the very infrared. For the extracted value of the running coupling in the infrared this leads to a distinct mismatch to what one is to expect on the basis of analytical results.

At first sight the fact that the power solution for the ghost dressing function could not be reproduced numerically to a reasonable precision may seem disappointing. Nevertheless these numerical results themselves show that the ghost dressing function is highly infrared singular. This reflects the long-range correlation of ghosts in Landau gauge. Therefore one should expect the ghost dressing function to be the one affected most by a finite volume. On the contrary the gluon dressing function vanishes in the infrared and consequently it is much less affected by a finite volume. We expect the ghost dressing function together with the running coupling to approach more and more the correct power solution in the infrared as lattice spacings are decreased and lattice sizes are increased.

Furthermore, we add a remark on the transversality of the gluon propagator as obtained in the bare vertex truncation scheme. Of course, the full gluon propagator calculated from the complete gluon equation with fully dressed vertices in Landau gauge is transversal due to Slavnov-Taylor identities. Thus such a hypothetical solution would be independent of the form of the projector, i.e. in our notation with the projector $(\delta_{\mu\nu}-\zeta p_\mu p_\nu)/p^2$ independent of the parameter ζ. In practice, using bare vertices as in our truncation scheme this is certainly not the case. Our numerical results for different values of the parameter ζ can be seen in Fig. 8. Although our solutions show the expected dependence on the form of the projector this dependence is not too drastic and in general the behavior of these different solutions is very similar.

For the gluon dressing function one observes that the more ζ grows the greater is the deviation from the pure power behavior. The points in the very infrared cannot be connected by a smooth line any more. Correspondingly this happens for the running coupling. Based on the infrared analysis one might anticipate that κ should approach the value $\kappa=0.5$ more and more as ζ grows until there is a jump to the solution from $\kappa=0.5^+$ to $\kappa=1$ as the Brown-Pennington limit $\zeta=4$ is reached. We do not observe such a qualitative jump in our solutions on a torus. The solution shown for $\zeta=4$ is approached smoothly when ζ approaches this limit. This clearly indicates that the solution $\kappa=1$ might not exist at all if one removes the torus as a regulator.

Finally we compare our results to recent SU(2) lattice calculations [31]. As has already been stated above the ghost and gluon dressing functions from Dyson-Schwinger equations are independent from the numbers of colors at least to our level of truncation. The only caveat in comparing our results with the lattice ones is the adjustment of the momentum scale which is certainly different from the case of SU(3) above. To get an appropriate momentum scale we therefore used the lattice result $\alpha_{SU(2)}(x)=0.68$ at $x=10\ \mathrm{GeV}^2$ as input. The two graphs in Fig. 9 show that the main qualitative features, the vanishing of the gluon and the divergence of the ghost dressing functions in the infrared, are common properties of both the lattice solutions and the one from Dyson-Schwinger equations. Even the power $\kappa=0.59\ldots$ of the gluon dressing function on the torus is very close to the one that can be extracted from the lattice fit to be $\kappa\approx 0.5$.

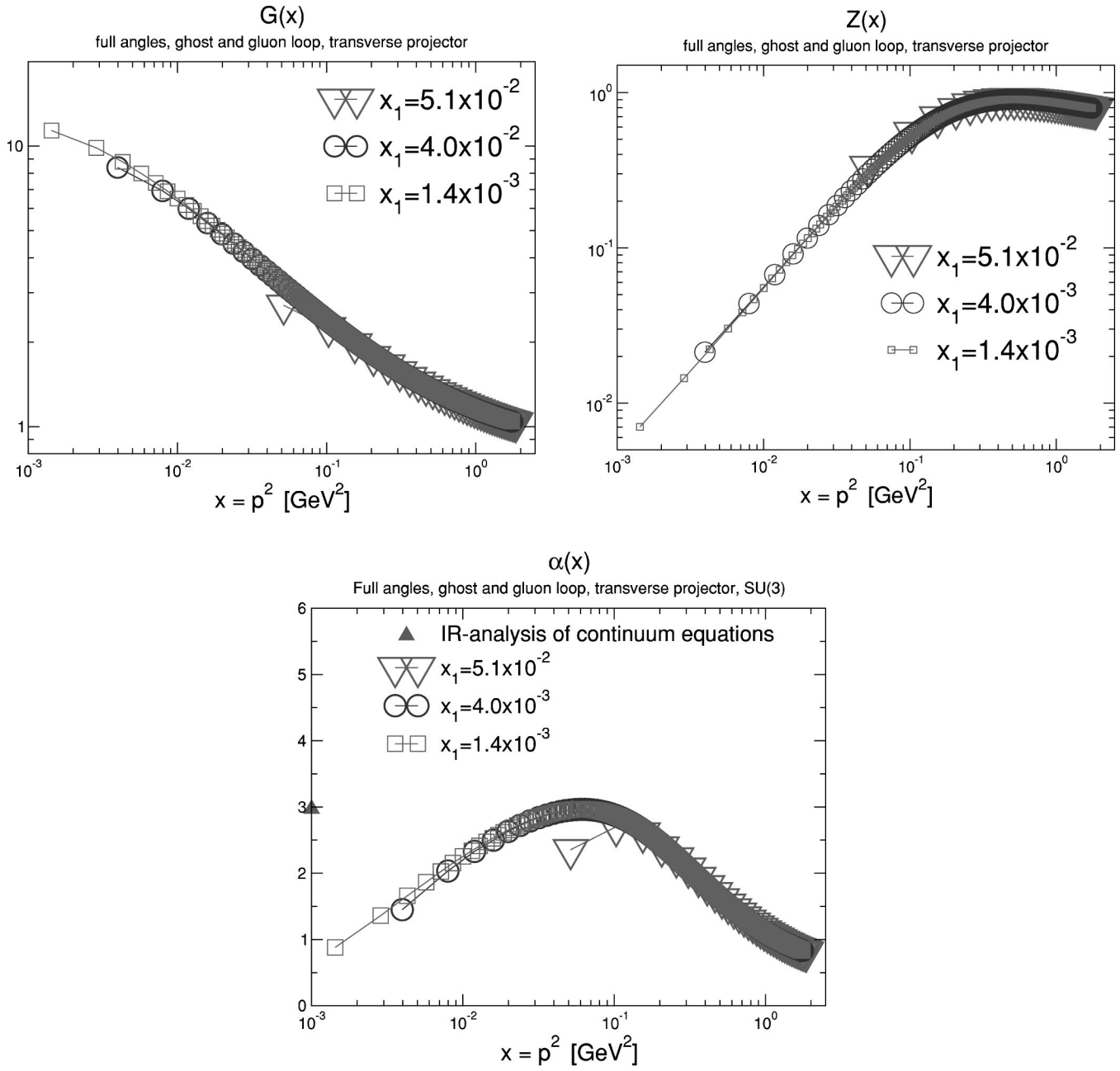

FIG. 7. Shown are the ghost dressing function, the gluon dressing function and the running coupling in the new truncation scheme without angular approximation for different volumes using a transverse projector.

The main difference of both approaches lies in the medium energy region around one GeV, where the Dyson-Schwinger solutions suffer from the missing two loop contributions that are certainly present in lattice Monte Carlo simulations.

V. CONCLUSIONS AND OUTLOOK

In this paper we have presented numerical solutions of truncated systems of Dyson-Schwinger equations for the gluon and ghost propagators in Landau gauge SU(N) Yang-Mills theories. We have employed a four-torus, i.e. a compact space-time manifold, as an infrared regulator. This enabled us to overcome angular approximations used so far in previous studies [3,4]. The basis for our numerical calculations have been provided by an analytic determination [6,7] of the exponents governing the infrared powerlike behavior of the gluon and ghost propagators. Typically the infrared analysis provide two possible values each for the gluon and the ghost, respectively. The central result of this paper is: Only one of these two possible infrared behaviors in a given truncation scheme can be matched to a numerical solution for nonvanishing momenta.

In a truncation scheme with a bare ghost-gluon vertex and a transverse projection of the (truncated) gluon equation this implies that the gluon propagator is only weakly infrared vanishing, $D_{gl}(k^2) \propto (k^2)^{2\kappa-1}$, $\kappa = 0.59\ldots$, and the ghost propagator is highly infrared singular, $D_{gh}(k^2) \propto (k^2)^{-\kappa-1}$. The running coupling possesses an infrared fixed point

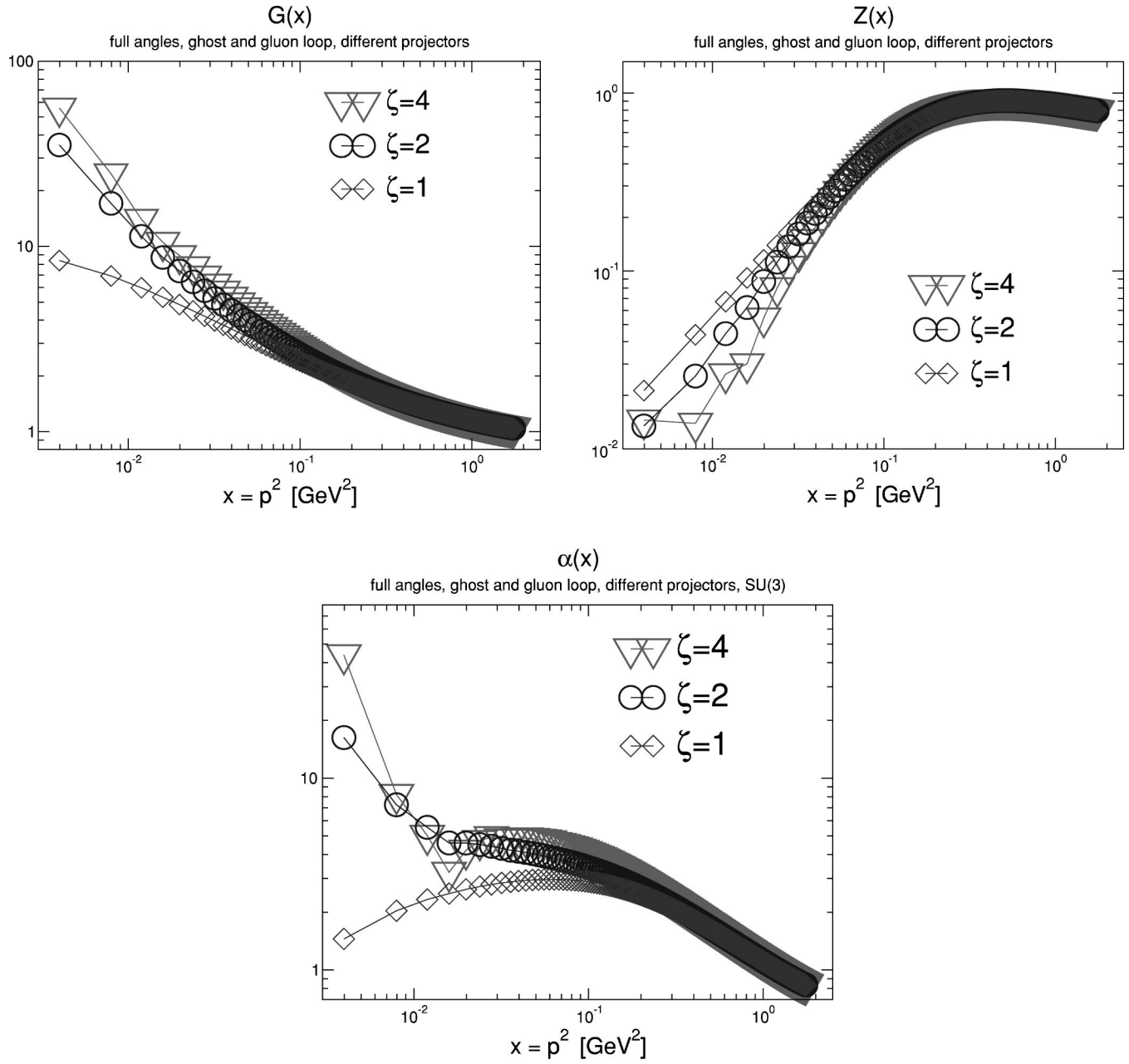

FIG. 8. The same as Fig. 7 for different projectors.

whose value is given by $\alpha(0)\approx 2.97$ [or, for a general number N_c of colors, $\alpha(0)\approx 8.92/N_c$].

Our results compare very favorably with results of recent lattice calculations performed for two colors. Due to the finite lattice volume the lattice results cannot, of course, be extended into the far infrared. In this respect our results are complementary to the lattice ones: We do obtain the infrared behavior analytically. On the other hand, lattice calculations include, at least in principle, all nonperturbative effects whereas we had to rely on truncations. E.g. the deviations for the gluon renormalization functions at intermediate momenta depicted in Fig. 9 might be due to the neglect of the four-gluon vertex function in our calculations.

As an outlook we would like to mention that employing a four-torus as an underlying manifold might serve for a number of interesting studies of Dyson-Schwinger equations. Amongst these, the use of twisted boundary conditions on the torus might enable one to shed some light on the importance of topologically nontrivial gauge field configurations for the infrared behavior of QCD Green's functions. We would like to note that recent lattice calculations [11] indicate a relation between the existence of center vortices in the maximal center gauge, the area law of the Wilson loop and the infrared behavior of the gluon propagator in Landau gauge.

Furthermore, we want to point out that choosing an asymmetric four-torus might provide an efficient mean to extend these calculations to nonvanishing temperatures. Here the main qualitative question arises about the fate of the Kugo-Ojima confinement criterion at the deconfinement transition.

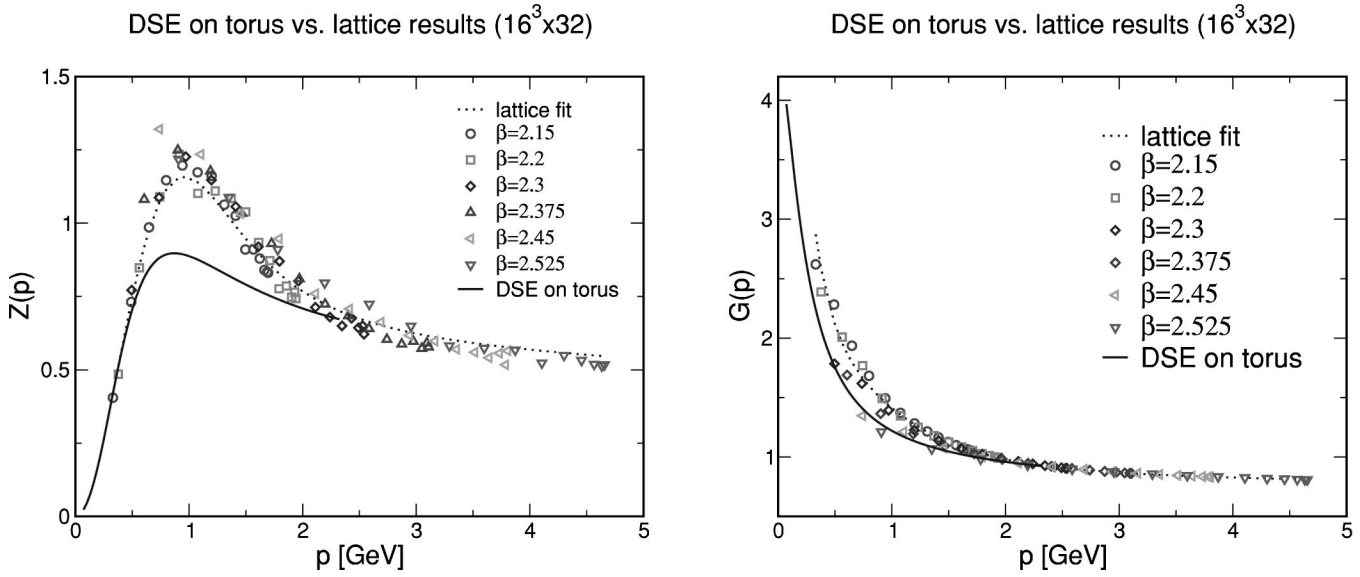

FIG. 9. Results on the torus compared to recent lattice results [31]. As the torus points are very close to each other on a linear momentum scale we did not resolve the torus curves into single points.

Finally, we want to remark that QCD Green's functions are an important input in many calculations in hadron physics [1,2]. The next necessary step towards such phenemenological applications is a study of the quark propagator. Such an investigation might hopefully also provide some insight into the mechanism of quark confinement in covariant gauges.

ACKNOWLEDGMENTS

We thank Jacques Bloch for many useful hints in the early stages of this work. We are especially grateful to Lorenz von Smekal for many valuable discussions and for making Ref. [7] available to us. We are indebted to Kurt Langfeld for communicating and elucidating his lattice results, partly prior to publication. Furthermore, we thank Sebastian Schmidt, Peter Watson, Andreas Wipf and Daniel Zwanziger for helpful discussions. This work has been supported by the DFG under contracts Al 279/3-3 and Re 856/4-1, and by the European graduate school Tübingen-Basel.

APPENDIX A: ONE-LOOP SCALING

In the framework of the truncation scheme presented in Sec. II C we have shown that the approximation

$$\mathcal{Z}_1(x,y,z;s,L)=\frac{G(y)^{(1-a/\delta-2a)}}{Z(y)^{(1+a)}}\,\frac{G(z)^{(1-b/\delta-2b)}}{Z(z)^{(1+b)}} \tag{A1}$$

for the gluon vertex renormalization constant yields the correct one loop scaling of the gluon loop in the gluon Dyson-Schwinger equation. This is true for any values a and b. Of course, in a full treatment of the coupled ghost gluon system $\mathcal{Z}_1(s,L)$ would be independent of momentum. Therefore a choice of a and b which keeps $\mathcal{Z}_1$ as weakly varying as possible seems the most reasonable one.

This choice can be inferred using the scaling of the dressing functions extracted from the renormalization group equation, see Ref. [3] for details. The dressing functions can be expressed as

$$Z(x)=\left(\frac{\alpha(x)}{\alpha(s)}\right)^{1+2\delta}R^2(x),$$

$$G(x)=\left(\frac{\alpha(x)}{\alpha(s)}\right)^{-\delta}R^{-1}(x), \tag{A2}$$

where the running coupling provides the correct one loop scaling in the ultraviolet. Consequently the function $R(x)$ approaches unity for high momenta. Furthermore, from the known infrared behavior of $Z(x)$, $G(x)$ and $\alpha(x)$ one infers that $R(x)$ is proportional to x^κ in the infrared. Writing $\mathcal{Z}_1$ in terms of $\alpha(x)$ and $R(x)$ yields

$$\mathcal{Z}_1(x,y,z;s,L)=\left(\frac{\alpha(\mu^2)}{\alpha(y)}\right)^{1+3\delta}R^{-3+a/\delta}(y)\times\left(\frac{\alpha(\mu^2)}{\alpha(z)}\right)^{1+3\delta}R^{-3+b/\delta}(z). \tag{A3}$$

In the perturbative region $R(y),R(z)\to 1$ and the function $\mathcal{Z}_1$ is therefore slowly varying for any a and b according to the logarithmic behavior of the running coupling α. In the infrared, however, α approaches its fixed point while the functions R behave like a power. Consequently the choice $a=b=3\delta$ guarantees the weakest momentum dependence of $\mathcal{Z}_1$ which is illustrated in Fig. 10. Shown is the y dependence of the function $\mathcal{Z}_1(x,y,z=y;s,L)$. [Note also that due to the symmetry $\mathcal{Z}_1(x,y,z;s,L)=\mathcal{Z}_1(x,z,y;s,L)$ and the absence of an explicit x dependence this is sufficient to demonstrate

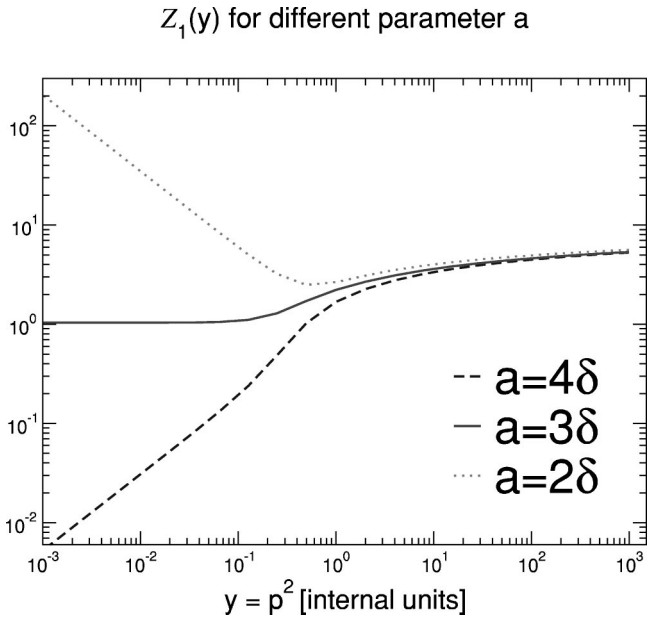

FIG. 10. The y dependence of the function $\mathcal{Z}_1(y,z)$ for different values of the parameter a. Only the choice $a=3\delta$ leads to momentum independence in the infrared. Due to the symmetry of the ansatz for $\mathcal{Z}_1(y,z)$ the z dependence is the same for $b=a$.

its momentum dependence.] In the perturbative momentum regime the function $\mathcal{Z}_1$ does not vary with the parameter a. So all three choices give the same logarithmic running in momentum as required to give the correct one loop scaling behavior of the integral. In the infrared, however, a change in a gives rise to substantial changes in the behavior of $\mathcal{Z}_1$, with only the choice $a=3\delta$ leading to a constant.

APPENDIX B: THE INFLUENCE OF ZERO MODES ON THE SOLUTIONS

An important point when formulating the Dyson-Schwinger equations on the torus could be the treatment of the zero modes. In addition, on the torus an infrared analysis like the one in flat Euclidean space-time is not possible, and one is left with the problem of how the dressing functions behave at vanishing momenta. Guided by the intuition that especially the long ranged modes should be affected by the finite volume we assume in the following $Z(x\to 0)=0$ just like in the continuum and $G(x\to 0)=\text{const}$ if zero modes are neglected. Phrased otherwise we assume that the zero modes are the missing ingredient to ensure the correct infinite volume limit for the torus results. Therefore, if on tori of different volumes $G(x=0)$ shows no sign of becoming divergent, the infrared enhancement seen in $G(x\to 0)$ or in the flat space-time results has to be due to the torus zero modes of gluons and ghosts.

Therefore, in this appendix, we will show that the assumption $G(x=0)<\infty$ does not lead to a contradiction in the equations on the torus if zero modes are neglected. To this end we focus on the truncation scheme without angular approximations. First we rewrite Eqs. (15),(16) as

$$\frac{1}{G(x)}=Z_3-g^2N_c\int\frac{d^4q}{(2\pi)^4}\frac{K(x,y,z)}{xy}G(y)Z(z), \quad \text{(B1)}$$

$$\frac{1}{Z(x)}=\tilde{Z}_3+g^2\frac{N_c}{3}\int\frac{d^4q}{(2\pi)^4}\frac{M(x,y,z)}{xy}G(y)G(z)+g^2\frac{N_c}{3}\int\frac{d^4q}{(2\pi)^4}\frac{Q(x,y,z)}{xy}\times\frac{G(y)^{-2-6\delta}}{Z(y)^{3\delta}}\frac{G(z)^{-2-6\delta}}{Z(z)^{3\delta}}. \quad \text{(B2)}$$

According to Appendix A we have chosen $a=b=3\delta$, where $\delta=-9/44$, the anomalous dimension of the ghost. The kernels have the form

$$K(x,y,z)=\frac{1}{z^2}\left(-\frac{(x-y)^2}{4}\right)+\frac{1}{z}\left(\frac{x+y}{2}\right)-\frac{1}{4}=xy\frac{\sin^2\Theta}{z^2}, \quad \text{(B3)}$$

$$M(x,y,z)=\frac{1}{z}\left(\frac{\zeta-2}{4}x+\frac{y}{2}-\frac{\zeta}{4}\frac{y^2}{x}\right)+\frac{1}{2}+\frac{\zeta}{2}\frac{y}{x}-\frac{\zeta}{4}\frac{z}{x}, \quad \text{(B4)}$$

$$Q'(x,y,z)=\frac{1}{z^2}\left(\frac{1}{8}\frac{x^3}{y}+x^2-\frac{19-\zeta}{8}xy+\frac{5-\zeta}{4}y^2+\frac{\zeta}{8}\frac{y^3}{x}\right)+\frac{1}{z}\left(\frac{x^2}{y}-\frac{15+\zeta}{4}x-\frac{17-\zeta}{4}y+\zeta\frac{y^2}{x}\right)-\left(\frac{19-\zeta}{8}\frac{x}{y}-\frac{3-4\zeta}{2}+\frac{9\zeta}{4}\frac{y}{x}\right)+z\left(\frac{\zeta}{x}+\frac{5-\zeta}{4y}\right)+z^2\frac{\zeta}{8xy}. \quad \text{(B5)}$$

We first analyze the behavior of the integrands in the limit $y\to 0$ for finite momenta x. Then $Z(z)\to Z(x)$ and $G(z)\to G(x)$ and the kernels times the respective dressing functions are to appropriate order in momentum y:

$$\frac{G(y)Z(z)}{xy}K(x,y,z)\to G(0)Z(x)\frac{\sin^2\Theta}{x^2}, \quad \text{(B6)}$$

$$\frac{G(y)G(z)}{xy}M(x,y,z)$$

$$\rightarrow G(0)G(x)\frac{1}{x^2}(1+(\zeta-2)\cos^2\Theta), \tag{B7}$$

$$\frac{G(y)^{-2-6\delta}G(y)^{-2-6\delta}}{Z(y)^{3\delta}Z(z)^{3\delta}xy}Q'(x,y,z)$$

$$\rightarrow\frac{G(0)^{-2-6\delta}G(x)^{-2-6\delta}}{Z(0)^{3\delta}Z(x)^{3\delta}xy}\left(\frac{\zeta\cos^2\Theta}{xy}+\cdots\right). \tag{B8}$$

Furthermore, $z=x+y-2\sqrt{xy}\cos\Theta$ has been used and terms proportional to $\cos\Theta$ have been dropped, as they either integrate to zero in the continuum or cancel each other in the sums on the torus. Each of the expressions (B6),(B7),(B8) is then the appropriate term for $j=0$ on the right-hand side of the Dyson-Schwinger equations on the torus. Clearly one observes that only a finite ghost mode $G(0)$ avoids trouble with divergencies. This is especially true for the kernel Q' of the gluon loop, as $Z^{-3\delta}(y\rightarrow 0)$ is more singular than the simple pole, so this kernel vanishes for small momenta y. The other two expressions (B6) and (B7) are finite. One is then left with the ambiguous quantities $\sin^2\Theta$ and $\cos^2\Theta$ which will be replaced by their integrals from zero to 2π in the calculation at the end of this section. The arbitrariness of this procedure is made considerably milder by the observation that any number plugged in for the trigonometric functions yields the same qualitative result at the end of this section.

Second, we take the limit $z\rightarrow 0$, which on the torus is identical to $\Theta\rightarrow 0$. The ghost kernel $\sin^2\Theta/z^2$ alone would certainly diverge as $\Theta\rightarrow 0$, but taking into account the power law behavior $Z(z)\sim z^{2\kappa}$ for the gluon dressing function the integrand is zero in this limit. This is valid for $\kappa>0.5$, which is in agreement with the infrared analysis in the continuum. We therefore may omit the points $z=0$ in the ghost equation. The situation is different in the gluon equation where the kernel of the ghost loop has a finite limit $z\rightarrow 0$: $M(x,x,0)/xy=(\zeta+1)/(2x^2)$. Therefore with a finite ghost dressing function $G(0)$ the points $z=0$ in the ghost loop contribute but no divergencies occur. In the gluon loop the kernel Q' multiplied by the dressing functions approaches zero for vanishing momentum z due to the power law behavior of $Z^{-3\delta}(z\rightarrow 0)$.

To obtain a definite value for $G(0)$ we now investigate the behavior of the equations (B1),(B2) in the limit $x\rightarrow 0$. The integrands are then given by

$$\frac{G(y)Z(z)}{xy}K(x,y,z)\rightarrow G(y)Z(y)\frac{\sin^2\Theta}{y^2}, \tag{B9}$$

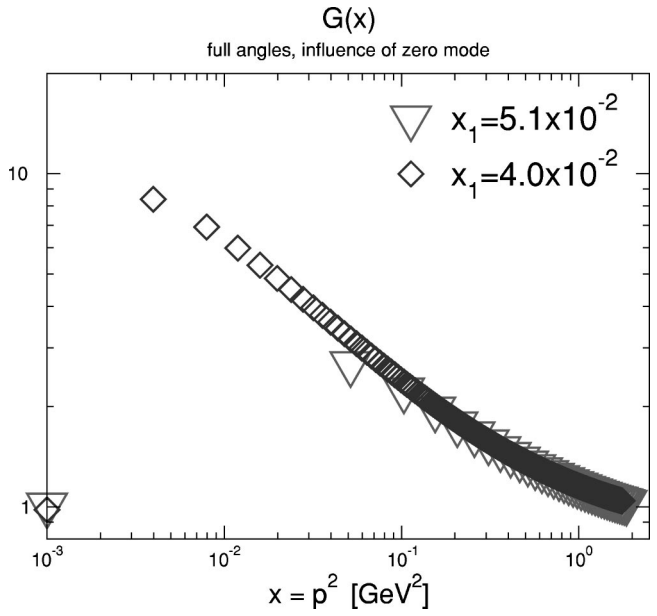

FIG. 11. The ghost mode $G(0)$ compared with the results for finite momentum x on the torus. For convenience we have kept the logarithmic momentum scale and plotted the zero modes on the left border of the figure.

$$\frac{G(y)G(z)}{xy}M(x,y,z)\rightarrow G(y)G(y)\left(\frac{1-\zeta\cos^2\Theta}{xy}+\cdots\right), \tag{B10}$$

where the kernel Q' is of no interest, as we know the gluon loop to be subleading in the infrared. Clearly, the kernel M of the ghost loop in the gluon equation is now singular for $x\rightarrow 0$, corresponding to a vanishing gluon dressing function in the infrared. This result confirms our working hypothesis that the gluon mode $Z(0)$ is not affected by the finite volume of the torus. The integrand of the ghost equation is finite up to the point $y=0$. There the pole in the kernel is canceled by the behavior of the gluon dressing function $Z(y)\sim y^{2\kappa}$ resulting in a zero for vanishing momentum x and y.

We therefore arrive at a consistent set of equations for a finite ghost mode $G(0)$ and a vanishing gluon mode $Z(0)$. In Fig. 11 we show the results for the ghost dressing function gained on two different volumes on the torus. Within numerical accuracy the values of $G(0)$ are the same for the two volumes. Obviously terms with high loop momentum y contribute most to the right-hand side of the ghost equation for vanishing momentum x. Furthermore, one observes that the actual value of $G(0)$ is not in accordance with an extrapolation of the ghost curves to the infrared. There is also no sizeable change of the gluon and the ghost dressing function when $G(0)$ is set to zero by hand. This has been done in all calculations in the main body of this paper.

Having shown that $G(0)<\infty$ on the torus even in the infinite-volume limit and assuming that the torus should provide a reasonable infrared regularization of physics in flat space-time we conclude that the divergence of $G(0)$ is very probably due to the torus zero modes of gluons and ghosts. Noting furthermore that a diverging $G(0)$ is related to the

Zwanziger-Gribov horizon condition and the Kugo-Ojima confinement criterion this indicates a direct relation between zero modes, the Gribov horizon and confinement.

APPENDIX C: NUMERICAL METHODS FOR FLAT EUCLIDEAN SPACE-TIME

The numerical methods to solve the coupled gluon-ghost system in flat Euclidean space-time after applying angular approximations has been described in great detail in Refs. [4,25]. Note that different numerical techniques have been employed in Refs. [3,25] and Ref. [4]. We have used all these techniques to verify the independence of our solutions from details of the numerical treatment.

First, we discuss the numerical renormalization process. As we know the characteristics of the solutions *a priori* we may exploit the possibility of independent subtractions of the gluon and the ghost equation. The procedure followed in Ref. [3] was to eliminate renormalization constants Z_3 and $\tilde{Z}_3$ by subtracting the equation at the renormalization scale $s=\mu^2$. The results presented in Sec. IV A are generated by solving the equations

$$\frac{1}{Z(x)}-\frac{1}{Z(s_Z)}=\frac{g^2N_c}{48\pi^2}\left(G(x)\int_0^x\frac{dy}{x}\left(-\frac{y^2}{x^2}+\frac{3y}{2x}\right)G(y)+\int_x^{\Lambda^2}\frac{dy}{2y}G^2(y)-G(s_Z)\int_0^{s_Z}\frac{dy}{s_Z}\left(-\frac{y^2}{s_Z^2}+\frac{3y}{2s_Z}\right)G(y)+\int_{s_Z}^{\Lambda^2}\frac{dy}{2y}G^2(y)\right), \tag{C1}$$

$$\frac{1}{G(x)}-\frac{1}{G(s_G)}=-\frac{9}{4}\frac{g^2N_c}{48\pi^2}\left(Z(x)\int_0^x\frac{dy}{x}\frac{y}{x}G(y)+\int_x^{\Lambda^2}\frac{dy}{y}Z(y)G(y)Z(s_G)\times\int_0^{s_G}\frac{dy}{s_G}\frac{y}{s_G}G(y)+\int_{s_G}^{\Lambda^2}\frac{dy}{y}Z(y)G(y)\right), \tag{C2}$$

for the truncation scheme of Sec. II B and analogous equations for the scheme of Sec. II A thereby introducing subtraction points s_Z and s_G. The parts of the integrals from $y=0$ to an infrared matching point ϵ are carried out analytically, with the dressing functions in the integral being replaced by their leading infrared behavior (32)

$$Z(x)=Ax^{2\kappa},\quad G(x)=Bx^{-\kappa}.$$

The infrared analysis leads to fixed values κ and $\alpha_c=\alpha(0)=(g^2N_c/12\pi)AB^2$, so A is left as a free parameter in the infrared expansion. For numerical reasons it is convenient to choose the subtraction points $s_G=0$ and s_Z to lie above the maximum of $Z(x)$. The two input parameters that determine the renormalization point where we require the normalization conditions $G(s=\mu^2)=Z(s=\mu^2)=1$ are then A and the value of the gluon dressing function at its subtraction point, i.e. $Z(s_Z)$.

The equations are solved using the Newton iteration method thereby generating values for the propagator functions. These are then plugged into the unsubtracted equations to obtain the respective values of the renormalization constants Z_3 and $\tilde{Z}_3$ for a given cutoff Λ and a given renormalization scale μ which allows us finally to determine the numerical solutions respecting the normalization conditions $G(s=\mu^2)=Z(s=\mu^2)=1$.

[1] R. Alkofer and L. von Smekal, Phys. Rep. **353**, 281 (2001).
[2] C.D. Roberts and S.M. Schmidt, Prog. Part. Nucl. Phys. **45**, S1 (2000).
[3] L. von Smekal, R. Alkofer, and A. Hauck, Phys. Rev. Lett. **79**, 3591 (1997); Ann. Phys. (N.Y.) **267**, 1 (1998).
[4] D. Atkinson and J.C. Bloch, Phys. Rev. D **58**, 094036 (1998); Mod. Phys. Lett. A **13**, 1055 (1998).
[5] P. Watson and R. Alkofer, Phys. Rev. Lett. **86**, 5239 (2001); R. Alkofer, L. von Smekal, and P. Watson, Proceedings of the ECT* Collaboration Meeting on Dynamical Aspects of the QCD Phase Transition, Trento, Italy, 2001, hep-ph/0105142.
[6] D. Zwanziger, Phys. Rev. D (to be published), hep-th/0109224.
[7] C. Lerche and L. von Smekal, hep-ph/0202194; C. Lerche, Diploma thesis, Erlangen University, 2001 (in German).
[8] J.E. Mandula, Phys. Rep. **315**, 273 (1999).
[9] F.D. Bonnet, P.O. Bowman, D.B. Leinweber, and A.G. Williams, Phys. Rev. D **62**, 051501(R) (2000).
[10] F.D. Bonnet, P.O. Bowman, D.B. Leinweber, A.G. Williams, and J.M. Zanotti, Phys. Rev. D **64**, 034501 (2001).
[11] K. Langfeld, H. Reinhardt, and J. Gattnar, Nucl. Phys. **B621**, 131 (2002); Nucl. Phys. B (Proc. Suppl.) **106**, 673 (2002).
[12] T. Kugo and I. Ojima, Suppl. Prog. Theor. Phys. **66**, 1 (1979).
[13] N. Nakanishi and I. Ojima, *Covariant Operator Formalism Of Gauge Theories And Quantum Gravity*, Lecture Notes in Physics Vol. 27 (World Scientific, Singapore, 1990).
[14] T. Kugo, International Symposium on BRS Symmetry, Kyoto, 1995, hep-th/9511033.
[15] L. von Smekal and R. Alkofer, Proceedings of the 4th International Conference on Quark Confinement and the Hadron Spectrum, Vienna, Austria, 2000, hep-ph/0009219.
[16] R. Oehme and W. Zimmermann, Phys. Rev. D **21**, 471 (1980); **21**, 1661 (1980).
[17] K. Nishijima, Czech. J. Phys. **46**, 1 (1996); M. Chaichian and K. Nishijima, hep-th/9909158, and references therein.
[18] D. Zwanziger, Nucl. Phys. **B364**, 127 (1991); **B399**, 477 (1993); **B412**, 657 (1994).
[19] V.N. Gribov, Nucl. Phys. **B139**, 1 (1978).
[20] D. Zwanziger, Nucl. Phys. **B209**, 336 (1982).

[21] P. van Baal, Nucl. Phys. **B369**, 259 (1992); talk given at NATO Advanced Study Institute on Confinement, Duality and Nonperturbative Aspects of QCD, Cambridge, England, 1997, hep-th/9711070.
[22] V.P. Gusynin, A.W. Schreiber, T. Sizer, and A.G. Williams, Phys. Rev. D **60**, 065007 (1999); A.W. Schreiber, T. Sizer, and A.G. Williams, *ibid.* **58**, 125014 (1998).
[23] L. von Smekal, P.A. Amundsen, and R. Alkofer, Nucl. Phys. **A529**, 633 (1991).
[24] N. Brown and M.R. Pennington, Phys. Rev. D **38**, 2266 (1988).
[25] A. Hauck, L. von Smekal and R. Alkofer, Comput. Phys. Commun. **112**, 149 (1998); **112**, 166 (1998).
[26] J.C. Taylor, Nucl. Phys. **B33**, 436 (1971).
[27] T. Muta, *Foundations of Quantum Chromodynamics* (World Scientific, Singapore, 1998), p. 409.
[28] J.C. Bloch, Phys. Rev. D **64**, 116011 (2001).
[29] G. 't Hooft, Nucl. Phys. **B153**, 141 (1979); P. van Baal, Ph.D. thesis, Utrecht, 1984, INIS-mf-9631.
[30] H. Reinhardt, Mod. Phys. Lett. A **11**, 2451 (1996).
[31] K. Langfeld (private communication).